Resistivity Device for Near Surface Studies

M. de la Vega[1], M. V. Bongiovanni[2] and V. Grünhut[3]

[1]GAIA (Grupo de Geofísica Aplicada y Ambiental, Buenos Aires University, IFIBA-CONICET, Argentina.

[2, 3] LIDTUA, Facultad de Ingeniería, Austral University, and CONICET, Argentina.

Corresponding author: María Victoria Bongiovanni (mbongiovanni@austral.edu.ar)

Key Points:

- DC resistivity device.
- Modular device.
- Open-source electronic platform.

Abstract

A programmable automated resistivity device was designed and constructed. The device was created to perform near surface studies, particularly archaeogeophysical target characterization. Field and physical model studies can be performed changing the current input of the device. The equipment consists of two independent devices, each one with its own microcontroller platform. They are interconnected through serial data transfer protocol. The first device, works as a resistivimeter where the ABMN electrode positions are programmed and permits the interaction with the user. The second one, connects the current and voltage channels to the programmed electrodes positions.

Different targets and electrode configurations such as dipole-dipole, Werner-Schlumberger and γ_{112} where tested in order to verify the performance of the automated resistivity device. The measurements give mean relative standard deviation values between 0.7% and 3.7% and data inversion convergence between 2.6% and 11%.

1 Introduction

The direct current resistivity technique is one of the most reliable geophysical prospection methods (Cheng et al., 2019). With this method, surface voltage differences produced by current flow in earth provide information about the resistivity distribution in the subsurface. 2D and 3D imaging obtained with this method is commonly used in different study areas: urban environmental prospection (Tsokas et al., 2011), tunnel detection (Orfanos and Apostolopoulos, 2011; Osella et. al., 2015; Simyrdanis et al., 2015), as an aid of archaeological studies (Bonomo et al., 2012), civil engineering studies (Martinelli et al., 2018), and contaminant plumes characterization (Ganiyu et al., 2015; Grünhut et al., 2018), surface-downhole measurements (Bergmann et al., 2012), etc.

With the development of faster hardware and more efficient software, it can be managed the increasingly number of data involved. Also, survey strategies can be modified interactively. With these advances, from the acquired data, reliable tomographies are obtained of the studied targets or sites.

Commercial and non-commercial (Bulgakov and Manshtein, 2006; Kutbay and Hardalac, 2017; Stummer et al., 2002; Zhe et al., 2007) resistivity automated multielectrode systems are basically of two types: centralized and distributed (Stummer et al., 2002). In the centralized systems, a unique controller through multiplexors open the different channels for current flow and voltage measurements. In the distributed systems, each electrode has the electronic necessary for the measurements.

We developed a programmable automated resistivity device. It was designed to study near surface geophysical targets in the field and on laboratory scale, which has required to handle two different current and voltage scales. The equipment was built in such a way that modules can be

added, for example allowing data transfer to the web. Another factor that we took into account in the design is that it can be extended with modules to handle a greater number of electrodes. A first version of the device can be seen in (de la Vega et al., 2019).

From the first years of the current century open source platforms are available that have been used for both basic and applied research (Mao et al., 2019). This coincides with the development of microcontroller platforms such as Arduino products (https://www.arduino.cc/) and single-board computers like the Raspberry Pi (https://www.raspberrypi.org/). This type of equipment allows to customize the application and to use adaptive monitoring or feedback and real-time control. Another advantage of these types of developments is that they enable a wide range of possibilities for user interaction. Sensor data can be transmitted from network-based data loggers to a web-based data exchange portal (Horsburgh et al., 2019). Equipment developed in this type of platform for environmental studies include for example CO2 monitoring (Blackstock et al., 2019) and water monitoring (Tziortzioti et al., 2019).

A centralized system is developed using an open-source electronic platform. The design and construction were performed taking into account Arduino platform capabilities. This platform, has a complete set of compatible modules to perform the different tasks of the device.

Different parts/functions of the device are managed by different processors interconnected via serial connection. The cables used are conventional. The electrodes, of galvanic contact, have no special design and multiple voltage measurements can be done with a single current shot for any electrode configuration via programming.

In the following sections we first describe the modular resistive device developed. Next, we present the laboratory tests performed in order to verify its performance. We show the inversion results with different configurations. Finally, the conclusions of the work carried out are exposed.

2 Resistive Device Design and Construction

The resistive device was designed in two independent hardware modules, each one with its own mainframe interconnected via serial protocol. In both units an Arduino Mega 2560 (ATmeg2560 microcontroller) is used as the processing unit. It has a cpu clock of 16 Mhz, 54 digital input/output pins with 5V logic and supports I2C and SPI as well as four serial facilities for communication with other devices. As power supply we used a commercial inverter of 220V powered by a 12V battery, whose signal was rectified by a diode bridge. It provides several output voltages: 100V, 75V, 50V, 25V and 12V.

The first device, the driver, is the main one. It works like a common resistivity device. It also points out to the second device, the automated platform, the electrode to be connected. The

automated platform acts as an intelligent relay matrix system that connects the different current and voltage channels to the electrodes where current is injected and voltage is measured.

The microcontroller of the driver device performs three different types of operations. The main function is to perform the current and voltage measurements. The second function is to control the different components that allow the user-device interaction. The third one is to send an order to the automated device with the information of which electrodes should be connected to the different current and voltage channels. Fig. 1 shows the block diagram of the resistive device.

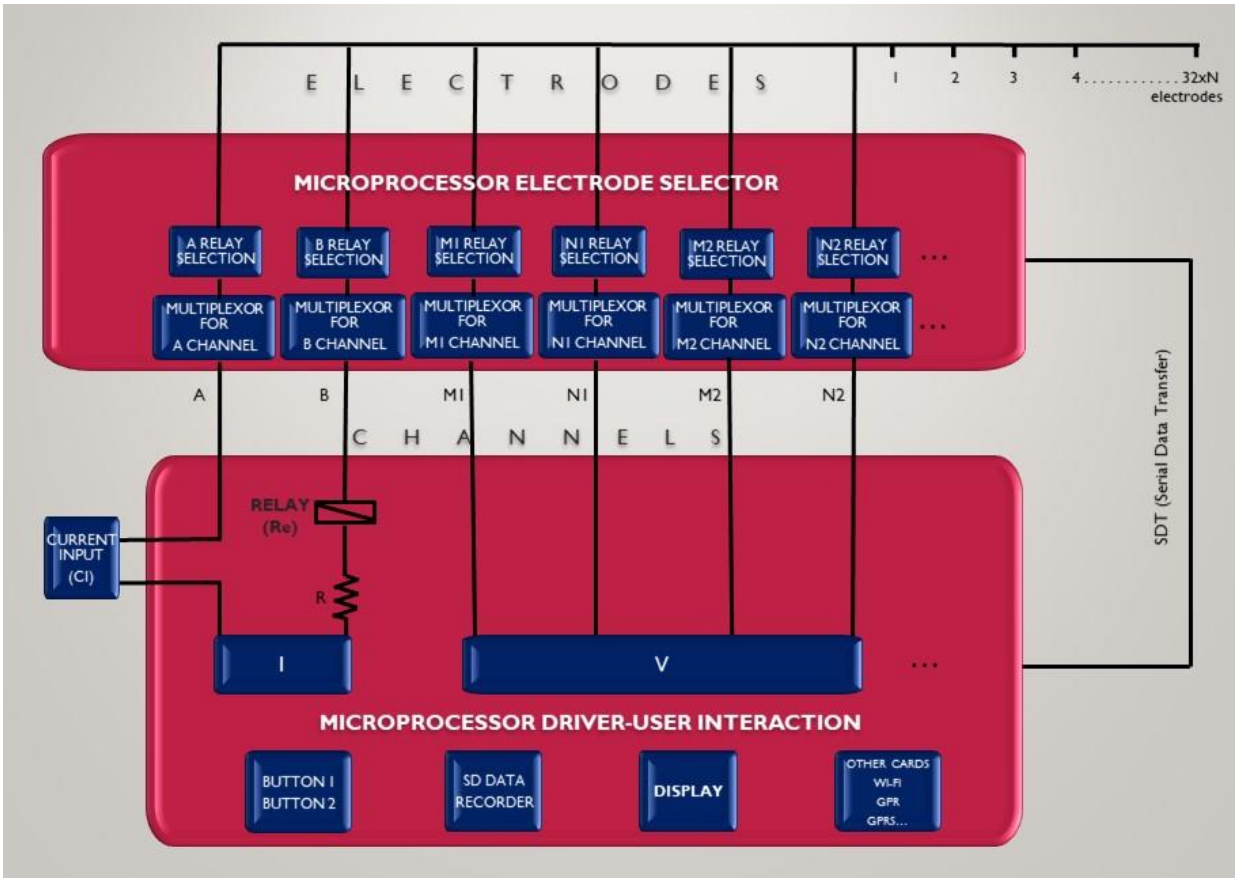

Figure 1. Block diagram of the resistivity device. Blue blocks are modules attached to the processors.

The current is measured with the Arduino compatible sensor INA 219 (I in Fig. 1 -channels A and B-) via the I2C bus. This sensor uses a shunt resistance of 0.1 ohm combined with a 12 bits analog digital converter (ADC). It can measure current between +-3.2A with a resolution of 0.8mA. Also it has a programmable gain amplifier (PGA) that can be programmed, for example, to measure currents between +-400mA with a resolution of 0.1mA. To the current circuit we attach a interchangeable limiting resistance (R) to be used with different current scales and a relay (Re) to start the current flow.

The voltage is measured with the analog digital converter ADS 1115 (V in Fig. 1 -channels M1, N1, M2 and N2-) that connects via the I2C bus. This board has a resolution of 16 bits (15 bits for the magnitude and one bit for the sign) and four channels which can be configured as two differential sensors. Four boards can be connected, using different addresses, configuring a system of eight differential channels. The voltage range of ADS1115 is +-6.144V. The resolution for this range is 0.1875mV. With the incorporated PGA set to gain one, the voltage range is +-4.096V with 0.125mV resolution.

The current source is external to the device (CI in Fig. 1). This current is adapted to the characteristic of the study to be made. The voltage and current ranges are modified by software while the limiting resistance is modified by hardware. Their values depend on the type of study we perform. For example, for near surface studies, we could use 50V as input with a limiting resistance of 100ohm, hence a maximum current of 0.5A can be obtained. For physical model studies we use 12V and 560ohm limiting resistance, therefore a maximum current of 0.02A is obtained. In both cases the current input is a square wave of period 200mS, and V and I are sampled with a frequency of 100samples/second. For each ABMN electrodes position five shots are made. This parameters are controlled by software that can be modified as needed.

In the first device, that commands the user-driver interaction, both the injection (A, B) and the voltage (M1, N1 M2, N2, etc.) electrodes positions are programmed. These configurations are programmed in the EEPROM memory of the microprocessor (4096 bytes available on Arduino Mega).

The user-device interfaces we implement to manage the equipment are: a SD card to record the data obtained, a LCD display to visually see the status of the equipment and a couple of buttons to select/start processes. Different electrode configurations kept in memory are selected via this buttons.

The automated device redirects the channels connected to the driver device to the appropriate electrodes. The information of the electrodes positions is obtained from the driver by serial transmission. Each channel is connected in the automated device to a multiplexor/demultiplexor (74HC4067) Arduino compatible module. Each multiplexor in turn is connected to a 16 relay board. This processor, once the electrodes positions received, indicates to each multiplexor which relay (electrode) has to be connected. In the constructed automated device each channel is connected to two multiplexor/relay board so 32 electrodes are available. This can be upgraded up to 256 electrodes. The electrodes are attached to the automated device using standard cables.

The overall operation of the system is as follows. After a setup protocol of both the Driver device microprocessor and the Automated device microprocessor, the user is asked to select one of the electrode configuration kept in the Driver´s memory. The electrodes positions are send to the

Automated device, which in turn connects the channels to the selected electrodes. After the Driver perform the resistivity measurements, the resulting data is send to memory and the next electrodes positions are send to the Automated. The loop continues until the last electrode position is measured and the data is saved in the SD card.

An example of the electrode position and output of the device is shown in Table 1. The first four columns show the position of the electrodes corresponding to a dipole-dipole configuration in the EEPROM memory of the Driver. Only one voltage measurement per current input (channel M1-N1) is programmed in this example. The last three columns show the output of the device kept in the SD card. Five measurements are made for each position of the electrodes.

Table 1

Example of Input - Output Data

Input Data				Output Data		
A	B	M1	N1	Measurement	ΔV/I	I
0	1	2	3	1	14.42	10.10
				1	14.24	10.40
				1	14.53	10.30
				1	14.22	10.30
				1	14.45	10.30
0	1	3	4	2	4.11	10.30
				2	4.00	10.30
				2	3.95	10.30
				2	3.88	10.30
				2	4.01	10.30
0	1	4	5	3	1.50	10.50
				3	1.38	10.30
				3	1.37	10.30
				3	1.41	10.50
				3	1.49	10.50
0	1	5	6	4	0.75	10.30
				4	0.61	10.10
				4	0.56	10.30
				4	0.67	10.30
				4	0.71	10.30
-	-	-	-	-	-	-
-	-	-	-	-	-	-
-	-	-	-	-	-	-
19	23	27	31	212	4.77	9.20

3 Performance of the device

In order to evaluate the performance of the constructed device we make target detection and characterization studies in physical models. In the tests we study localized and extended targets in 2D and 3D using different configurations.

First we studied a sphere submerged in salt water. We perform 2D tomographies of it using dipole-dipole, Wenner-Schlumberger, and γ_{112} (plus mirror) configurations. We also show the results obtained of a 3D tomography of the sphere using dipole-dipole configuration.

Next we study a distributed target, a hollow plastic tube with closed ends immersed in the same medium than in the previous experiment. We present the 2D and 3D tomographies obtained with dipole-dipole electrode configuration using the resistivity device.

The targets studied with the resistivity device are submerged in a plastic container filled with saltwater of horizontal dimensions 35cmx25cm and12cm height. The targets are placed in a region of dimensions 15cmx15cm in the central part of the box to eliminate boundary contributions. The targets are about 3cm diameter and around 1cm from the water surface. As the resolution obtained with the geoelectric method is about half the electrode separation, 16 electrodes 1cm apart were used. In Fig. 2 it can be seen a photo of the physical model and the device prepared for the sphere study.

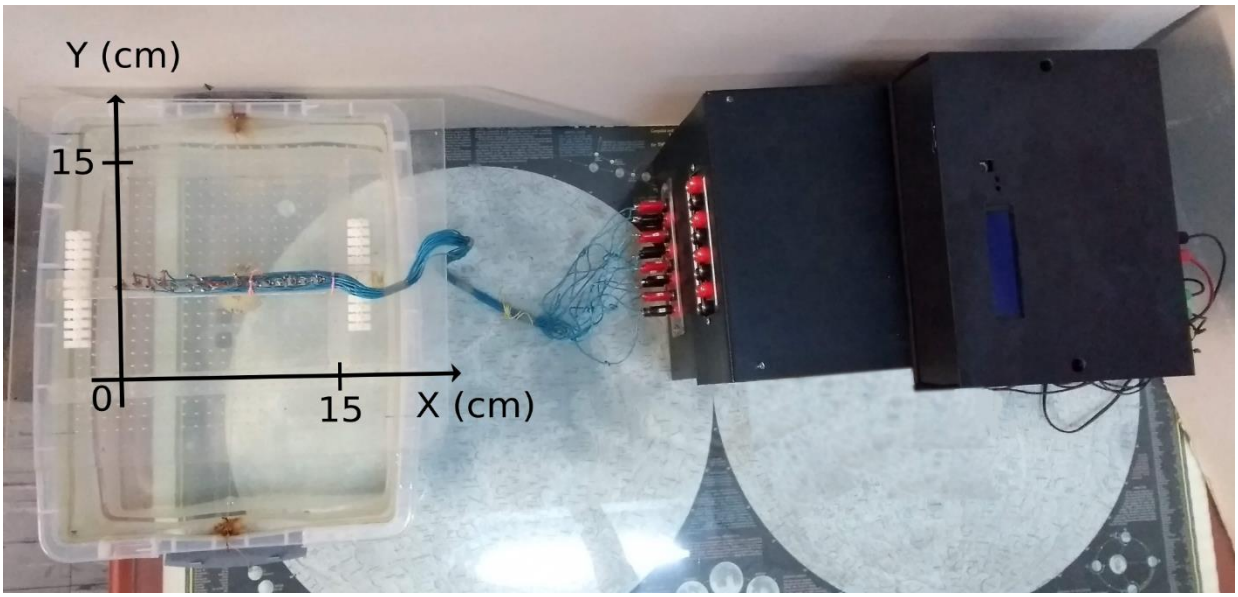

Figure 2. Photo of the physical model and the device prepared for the sphere study. The coordinate system taken in the study area is displayed.

193
194 To prevent electrolysis effects a low current input was used. This is generated using 12V input
195 and a limiting resistance of 560ohm then a maximum current of 0.02A is achieved.
196
197 For this configuration, the voltage ADC PGA is set to gain one: the voltage range is +-4.096V
198 with 0.125mV resolution. The current PGA is programmed to measure currents between +-
199 400mA with a resolution of 0.1mA. The device was programmed to take five measurements in
200 each A, B, M1, N1 position (only one differential voltage was measured at a time) and record the
201 time evolution of voltage/current at each A B M1 N1 positions.
202
203 An example of the time evolution of an individual measurement made in the physical model is
204 shown in Fig. 3a. A dipole-dipole configuration was taken with a = 1cm and n = 3. From this
205 graph, we obtain a $\Delta V/I$ mean value of 1.563ohm a and relative standard deviation of 0.6%. For
206 comparison, we also show in Fig. 3b an equivalent measurement performed on the ground
207 changing the 1cm scale to 1m, using an input voltage of 50V, and a limiting resistance of
208 100ohm. From this graph we obtain a $\Delta V/I$ mean value of 0.133ohm and a relative standard
209 deviation of 0.9%. Furthermore, physical models tomographies give similar results over all
210 relative standard deviation of the $\Delta V/I$ data obtained (see sections 3.1 and 3.2).
211

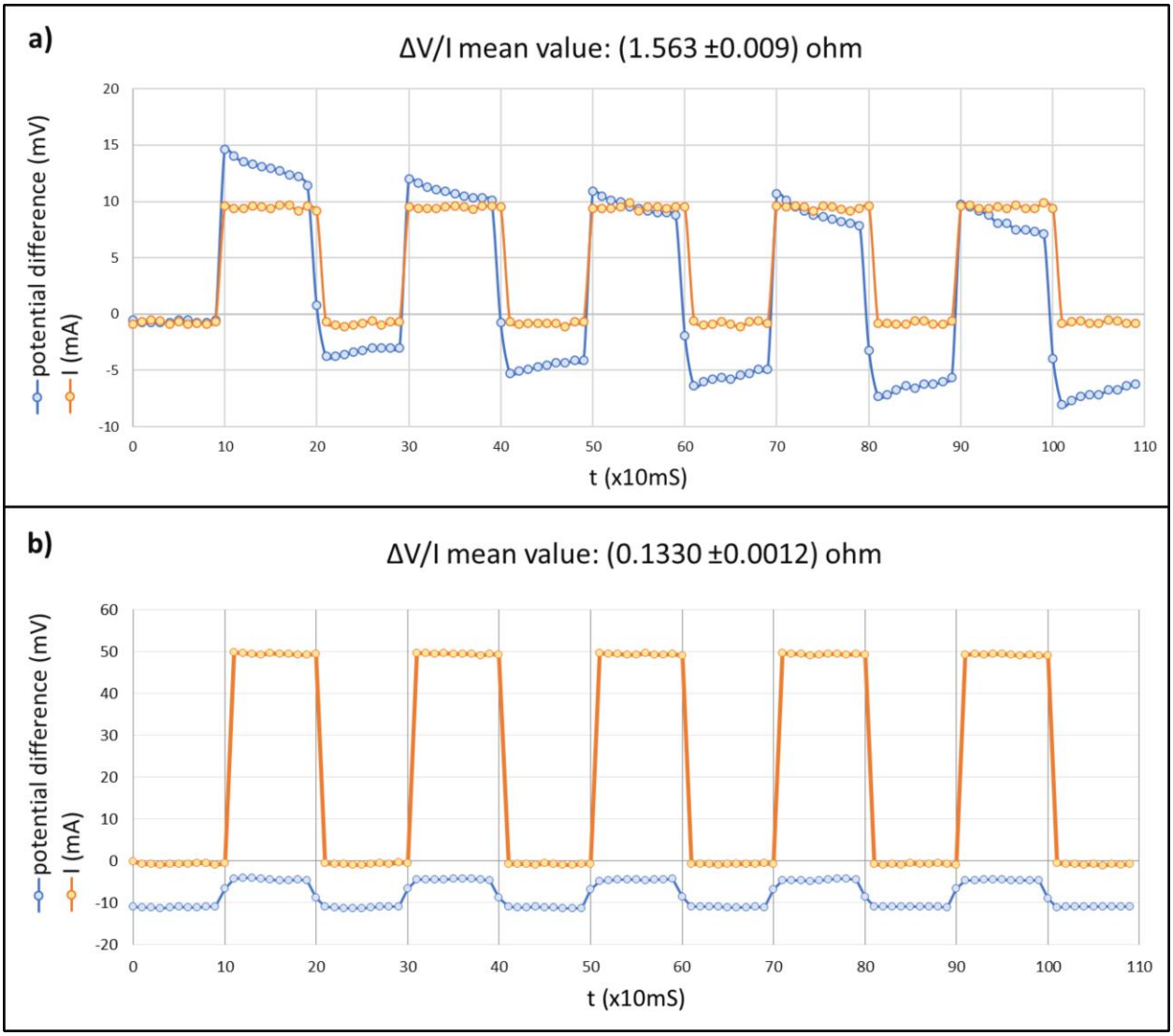

Figure 3. Time evolution of signals; potential difference (mV) and I (mA) a) in the laboratory, b) in the field.

3.1 Sphere target detection study

The studied sphere is of 4cm diameter, submerged at 0.5cm from the saltwater top surface and centred in the horizontal plane.

We have programmed the electrodes positions to make in-line dipole-dipole (D-D), Schlumberger-Wenner (S-W) and γ_{112} plus mirror configuration profiles as shown in Table 2. This last electrode configuration was included due to its efficiency to characterize localised targets with few measurements (Szalai et al., 2015).

Table 2

Configurations Programmed In The Device

Config.	Measurements	nmax	a	Electrode Distribution
D-D	106	6	1,2,3,4	A-a-B-na-M-a-N
S-W	80	6	1,2,3	A-na-M-a-N-nB
γ_{112}	48		1,2,3,4,5	A-a-M-a-B-2a-N
				N-2a-B-a-M-a-A

The mean relative standard deviation of the 106 dipole-dipole measurements is 3.76%, with a minimum of 0.2% and a maximum of 37%. For the 80 Schlumberger-Wenner measurements the values are, mean: 0.7%, minimum: 0.2% and maximum: 1.4%. The values for the 48 γ_{112} and mirror measurements are, mean: 1.0%, minimum: 0.2% and maximum: 11%. The high error value of dipole-dipole measurement comes from the n = 6 contribution, the value from the low voltage differences.

In the following figures we can see the inversion results of the configurations mentioned above. They were performed using the BERT (boundless electrical resistivity tomography) package (Günter et al., 2006). In all the cases, was considered the error that comes from the dispersion of the measured data. An anisotropy factor of 0.1 was assumed for the smoothness constraints. The parameters were successively determined by doing inversions for which single parameters were varied. The regularization parameter, λ, had to be chosen properly. Data were inverted using several different regularization parameters ranging from λ = 5 to 300 and using the robust L1 norm. For the interpretation we choose the model for which the inversion achieved an acceptable error (λ = 5 for the S-W configuration and λ = 300 for the γ_{112} and D-D configurations). The quality of the inversion of ERT data was determined by the value of the RRMS (Relative Root Mean Square) and the χ^2 (Günter et al., 2006). In practice, values close to 1 for the chi-squared misfit show reliable results.

Fig. 4 shows the results of the D-D configuration. The resistive ball can be perfectly distinguished, and the convergence is very good; i.e., the RRMS deviation was 8% and χ^2 = 0.95. Fig. 5 shows the results of the S-W configuration. Although the ball can be distinguished and the convergence is very good (RRMS 2.6%, χ^2 = 0.79), in this case the deepest zone could not be resolved as well as in D-D case. Fig. 6 shows the results of γ_{112} configuration. The convergence is also good (RRMS 11%, χ^2 = 0.98). Although qualitatively the ball can be distinguished, the resolution was not so good. This can be due to the fact that γ_{112} configuration proved to be more successful in comparison with the traditional configurations if the contrast was small (160-140 ohm.m), and also where the target is at a relatively large depth, which is not our case (Szalai et al., 2015).

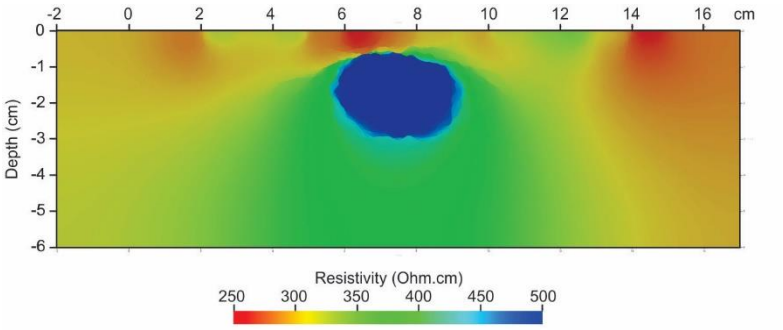

Figure 4. D-D data inversion result.

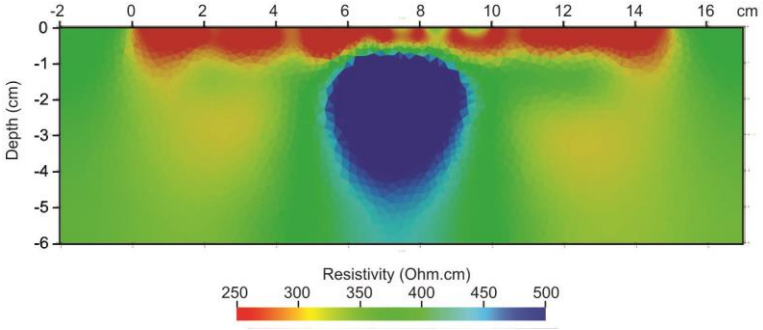

Figure 5. S-W data inversion result.

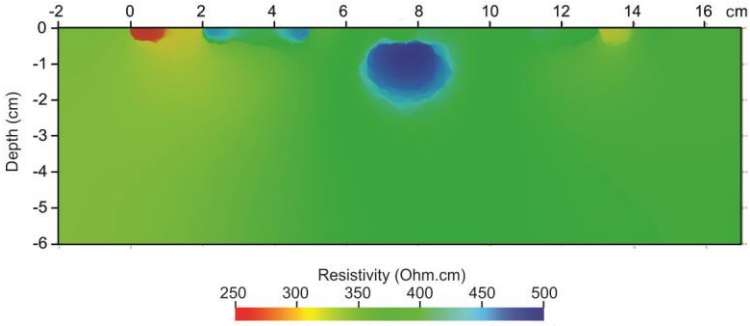

Figure 6. γ_{112} data inversion result.

We also performed 3D measurements in the container using the same sphere but with the medium less conductive than in the previous case. The sphere was submerged at 0.5cm from the saltwater top surface and centered in the horizontal plane. We performed sixteen dipole-dipole profiles along X axis every 1cm, and six profiles along Y axis separated 3cm. In each profile, sixteen electrodes were used with 1cm separation between them. The data was inverted using also the BERT package. In Figs. 7a and 7b the D-D tomography obtained is displayed. The resistive ball is perfectly reproduced and the convergence is good (RRMS 11.3%, χ^2 = 0.94) despite the fact that the resistive contrast between the ball and the water is not as large as in the previous case.

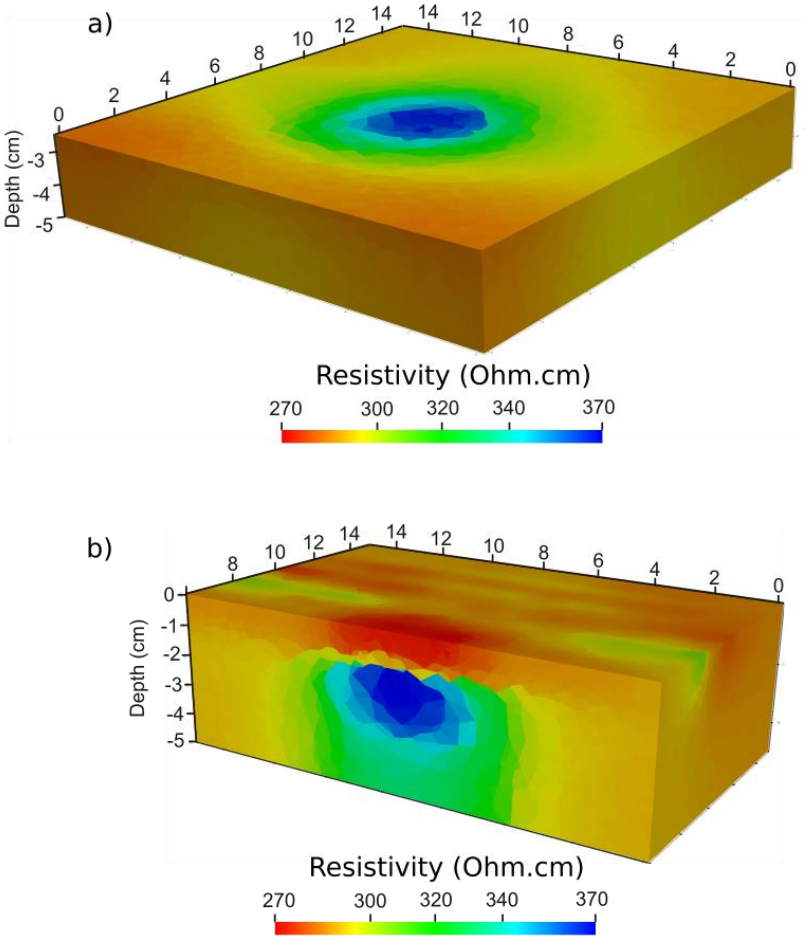

Figure 7. 3D data inversion result. **a)** Top view, **a)** Lateral view.

3.2 Tube target detection study

Next, we study the performance of a device detecting a hollow plastic tube with closed ends submerged in the same container than in the previous experiment, filled also with saltwater. This physical model was carried out as part of the research that we have begun in previous years, in relation to the alleged presence of tunnels in the Avellaneda Park, Buenos Aires (Bongiovanni et al., 2018).

A 3cm diameter tube was submerged with a slight inclination both with respect to the horizontal (XY) plane and with respect to the perpendicular (XZ) plane. The total length of the tube is

20cm. Into the study zone, the center of the tube intersects the X axis at X=6cm, Y=0cm according to the coordinate system shown in the Fig. 4., submerged at approximately 1.3cm. The center of the tube intersects X = 9cm at Y =15cm, and was submerged at 1.7cm. We performed sixteen dipole-dipole profiles along the direction of the tube (Y axis) every 1cm, and three profiles in the crossing direction (X axis) separated 4cm. In each profile, sixteen electrodes were used with 1cm separation between them.

As in the previous experiment, the 2D lines were inverted using the BERT software. We show three representative lines where it can be appreciated the localization of the tube. Fig. 8 shows one end, Y = 0 cm. The RRMS deviation was 7.5% and χ^2 = 0.97. In Fig. 9 we can see the other end, Y = 15, with RRMS 4.89% and χ^2 = 0.97. In this two lines the localization of the tube was well reproduced. In Fig. 10 we show the line X = 7, which is parallel to the length of the tube. The RRMS deviation was 2.9% and χ^2 = 5.9. In this case, the convergence was not so good, but the tube could be detected and located properly.

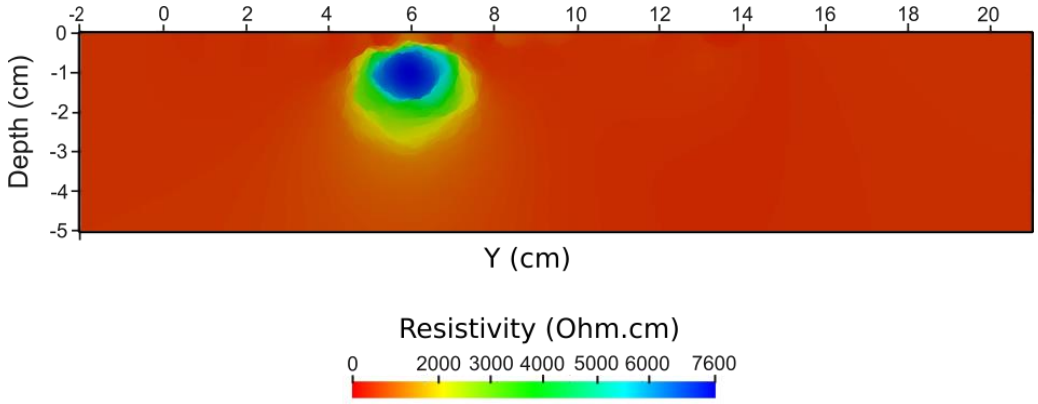

Figure 8. Line Y = 0 cm data inversion result.

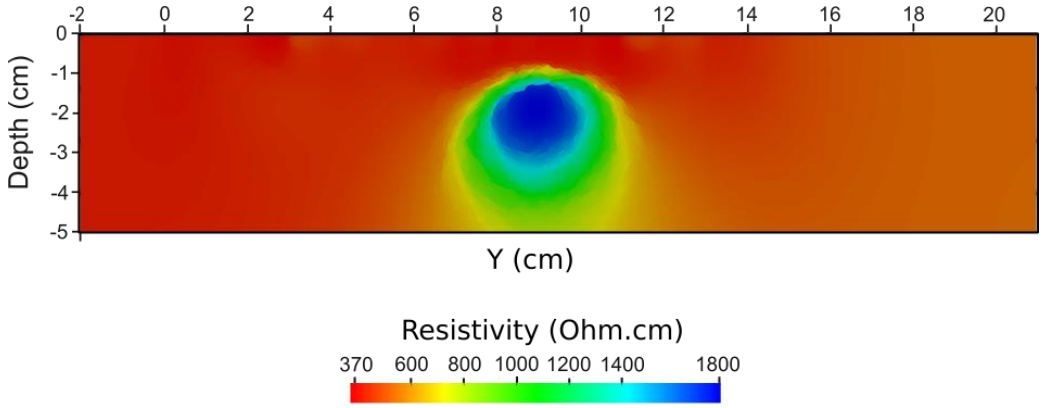

Figure 9. Line Y = 15 cm data inversion result.

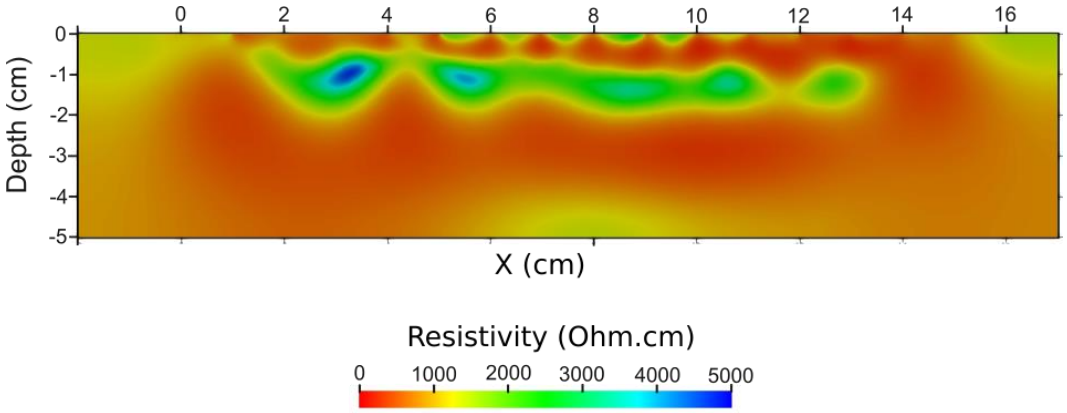

Figure 10. Line X = 7 cm data inversion result.

The 3D data was inverted also using the BERT package. In Fig. 11 the D-D tomography obtained is displayed. The resistive tube is well reproduced and the convergence is good (RRMS 4.8%, χ^2 =1.4).

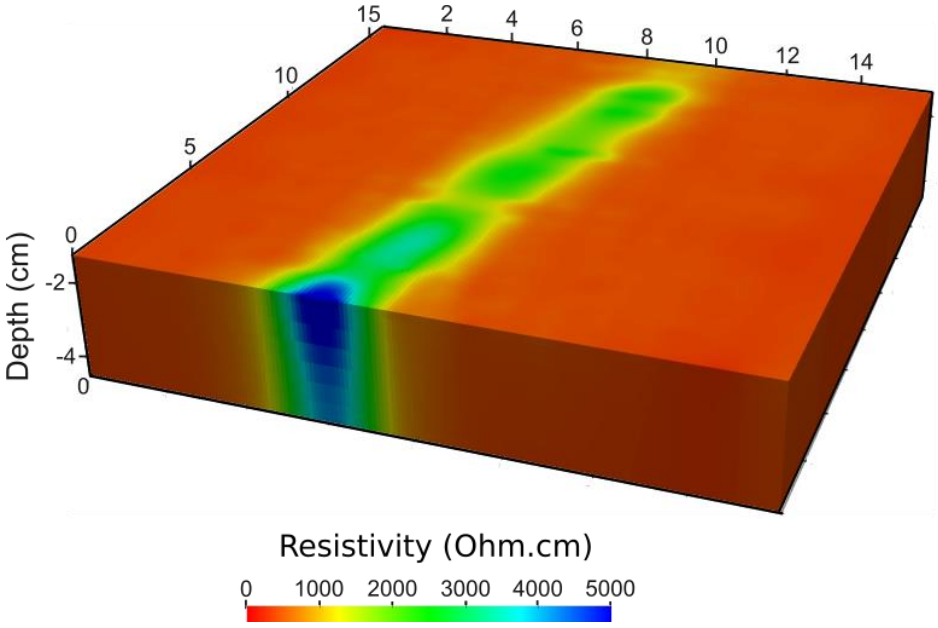

Figure 11. 3D data inversion result.

4 Conclusions

The individual measurements of voltage and current time evolution performed with the device yielded good results as the standard deviations obtained were small. Furthermore, the measurements were well correlated between them as the inversion tomographies obtained were in agreement with the model.

Regarding the experiment with the ball, the 2D resistivity tomographies obtained in the D-D and S-W configurations have adequately reproduced the physical model. This shows that the equipment is working properly, with a fine resolution power. In the case of γ_{112} configuration, although the ball can be distinguished, the resolution was not so good. We think this can be due to the electrode configuration itself and/or to the inversion procedure. Numerical investigations showed that γ_{112} configuration is more meaningful in cases where the resistivity contrast is smaller than in our case, and in cases of deeper targets. Also can be brought out by the fact that the current and potential electrodes are intercalated. Regarding the experiment with the tube, the 2D tomographies obtained also have adequately reproduced the physical model. The 3D reconstruction both of the ball and the tube also shows an excellent agreement with the model although the inversion convergence was bigger. This confirms the good resolution that can be achieved with the device. We plan to use this device to continue research on the presence of tunnels in Parque Avellaneda, an area in the city of Buenos Aires. Future development plans also include both the possibility of using this device in IP studies, as well as adding a module that allows real-time experiments, transferring the data to the web.

Acknowledgments

This work was partially supported by CONICET (National Scientific and Technical Council Research) and ANPCyT (National Agency for Scientific and Technological Promotion), Argentina.

The authors want to thank Ana Osella for their constructive comments, and Ernesto López for their assistance in carrying out valuable details in the construction of the physical model.

The supplemental files may be accessed from a permanent repository at 10.5281/zenodo.4268774.

References

Bergmann, P., Schmidt-Hattenberger, C., Kiessling, D., Rücker, C., Labitzke, T., Henninges, J., Baumann, G. & Schütt, H. (2012). Surface-downhole electrical resistivity tomography applied to monitoring of CO2 storage at Ketzin, Germany, *Geophysics*, Vol. 77, no. 6 pp. B253–B267, 2012. doi.org/10.1190/geo2011-0515.1

Blackstock, J. M., Covington, M. D., Perne, M., & Myre, J. M. (2019). Monitoring atmospheric, soil, and dissolved CO_2 using a low-cost, Arduino monitoring platform (CO2-LAMP): theory, fabrication, and operation. *Frontiers in Earth Science* 7, 313. doi:10.3389/feart.2019.00313

Bongiovanni, M., Grünhut, V., Martinelli, P., de La Vega, M., & Bonomo, N. (2018). *Geoelectrical and EMI studies at an urban site in Buenos Aires, Argentina, for localizing an old*

tunnel. Paper presented at Conference Proceedings and 24th European Meeting of Environmental and Engineering Geophysics, Porto, Portugal. p 1–5. doi:10.3997/2214-4609.201802618

Bonomo, N., Osella, A., Martinelli, P., de la Vega, M., Cocco, G., Letieri, F., & Frittegotto, G. (2012). Location and characterization of the sancti spiritus fort from geophysical investigations. *Journal of Applied Geophysics* 36, 57–64. doi:10.1016/j.jappgeo.2012.04.005

Bulgakov, A. Y. & Manshtein, A. K. (2006). A geophysical device for automation of multielectrode electrical prospecting. *Instruments and Experimental Techniques* 49:4, 565–567. doi:10.1134/S002044120604021X

Cheng, Q., Tao, M., Chen, X., & Binley, A. (2019). Evaluation of electrical resistivity tomography (ERT) for mapping the soil–rock interface in karstic environments. *Environmental Earth Sciences* 78. doi:10.1007/s12665-019-8440-8

de la Vega, M., Bongiovanni, M. V. y Osella, A. (2019). *Modular resistivity device for physical model studies*. Paper presented at Conference Proceedings, 25th European Meeting of Environmental and Engineering Geophysics, The Hague, The Netherlands. p.1 – 5. doi.org/10.3997/2214-4609.201902416

Ganiyu, S. A., Badmus, B. S., Oladunjoye, M. A., Aizebeokhai, A. P., & Olurin, O. T. (2015). Delineation of leachate plume migration using electrical resistivity imaging on lapite dumpsite in Ibadan, Southwestern Nigeria. *Geosciences* 5, 70–80. doi:10.5923/j.geo.20150502.03

Grünhut, V., Bongiovanni, M. V., & Osella, A. (2018). Using surface downhole ERT for detecting contaminants in deep aquifers due to the exploitation of oil reservoirs. *Near Surface Geophysics* 16, 545–556. doi:10.1002/nsg.12008

Günter, T., Rücker, C., & Spitzer, K. (2006). Three-dimensional modeling and inversion of dc resistivity data incorporating topography – part II: inversion. *Geophysical Journal International* 166, 506–517. doi:10.1111/j.1365-246X.2006.03011.x

Horsburgh, J., Caraballo, J., Ramírez, M., Aufdenkampe, A., Arscott, D., & Damiano, S. (2019). Low-cost, open-source, and low-power: But what to do with the data? *Frontiers in Earth Science* 7:67, 1–14. doi:10.3389/feart.2019.00067

Kutbay, U. & Hardalac¸, F. (2017). Development of a multiprobe electrical resistivity tomography prototype system and robust underground clustering. *Expert Systems* 34:e12206. doi:10.1111/exsy.12206

Mao, F., Khamis, K., Krause, S., Clark, J., & Hannah, D. M. (2019). Low-cost environmental sensor networks: recent advances and future directions. *Frontiers in Earth Science* 7, 221. doi:10.3389/feart.2019.00221

Martinelli, P., Osella, A., de la Vega, M., & Pinio, A. (2018). Different techniques for the assessment of geoelectrical data errors to improve the electrical images obtained at an industrial plant. *Near Surface Geophysics* 238-256, 16. doi:10.1002/nsg.163001

Orfanos, C. & Apostolopoulos, G. (2011). 2D–3D resistivity and microgravity measurements for the detection of an ancient tunnel in the Lavrion area, Greece. *Near Surface Geophysics* 9, 449–457. doi:10.3997/1873-0604.2011024

Osella, A., Martinelli, P., Grunhut,¨ V., de la Vega, M., Bonomo, N., & Weissel, M. (2015). Electrical imaging for localizing historical tunnels at an urban environment. *Journal of Geophysics and Engineering* 12, 674–685. doi:10.1088/1742-2132/12/4/674

Simyrdanis, K., Tsourlos, P., Soupios, P., Tsokas, G., Kim, J.-H., & Papadopoulos, N. (2015). Surface-to-tunnel electrical resistance tomography measurements. *Near Surface Geophysics* 13, 343–354. doi:10.3997/1873-0604.2015019

Stummer, P., Maurer, H., Horstmeyer, H., & Green, A. G. (2002). Optimization of dc resistivity data acquisition: Real-time experimental design and a new multielectrode system. *IEEE Transactions on Geoscience and Remote Sensing* 40:12, 2727 – 2735. doi:10.1109/TGRS.2002.807015

Szalai, S., Lemperger, I., Metwaly, M., Kis, A., Wesztergom, V., Szolokili, V., & Novák, A. (2015). Increasing the effectiveness of electrical resistivity tomography using γ_{11n} configurations. *Geophysical Prospecting* 63, 508–524. doi:10.1111/1365-2478.12215

Tsokas, G. N., Tsoulos, P. I., Vargemezis, G., & Pazaras, N. (2011). Using surface and cross-hole resistivity tomography in an urban environment: An example of imaging the foundations of the ancient wall in Thessaloniki, North Greece. *Physics and Chemistry of the Earth* 36, 1310–1317. doi:10.1016/j.pce.2011.03.007

Tziortzioti, C., D. Amaxilatis, I. M., & Chatzigiannakis, I. (2019). IoT sensors in sea water environment: Ahoy! experiences from a short summer trial. *Electronic Notes in Theoretical Computer Science* 343,117–130. doi:10.1016/j.entcs.2019.04.014

Zhe, J., Greenhaigh, S., & Marescot, L. (2007). Multichannel, full waveform and flexible electrode combination resistivity-imaging system. *Geophysics* 72:2, F57–F64. doi:10.1190/1.2435081